Lens induced by stress in optical windows for high-pressure cells

D. P. Shelton
Department of Physics, University of Nevada, Las Vegas, Las Vegas, Nevada 89154

(Received 10 March 1992, accepted for publication 28 April 1992)

Calculations are described of the elastic stress, strain, and surface displacement for a high-pressure optical window consisting of a transparent cylinder which is supported on a flat seat with an axial hole (Poulter window). Under pressure the window is compressed, and its outside surface bulges through the hole in the support. The net optical effect is to create a weak positive lens and to increase the axial optical thickness of the window.

I. INTRODUCTION

Optical measurements of gases require windows to seal the optical measurement cell. Usually, transmission of the required light and operation without breakage are the only important criteria for the windows.[1] However, laser, interferometric, and nonlinear optical measurements can impose additional, more stringent requirements on the windows. In particular, the results obtained for the nonlinear optical susceptibilities of gases by means of harmonic generation measurements are very sensitive to changes in focusing or optical power of the fundamental laser beam. In order to obtain accurate results, one must either eliminate or else quantitatively account for the changes in laser beam focusing and transmission that occur when the measurement cell is filled with gas. Since the calibration of the currently most accurate nonlinear-optical susceptibility measurements requires comparison of helium gas at 100 atm with other gases at much lower pressures, it is important to assess the possible systematic errors that may arise due to the effects of high gas pressure on the windows of the gas cell.[2] The gas cell in those experiments is closed at each end by a thick cylindrical glass window resting on a support plug with a flat, optically polished face. The laser beam passes through an axial hole in the support plug. Such an arrangement, known as a Poulter window, is widely used for optical high-pressure cells.[1,3] An accurate assessment of the optical effects of pressure on windows of this type can be obtained from a theoretical calculation because of the simple geometry, and because it is possible to produce actual windows and seats which adequately conform to the geometrical ideal. Accordingly, we have carried out calculations of the linear elastic deformation, strain, and stress of a Poulter window. The optical effects of pressure on the window are calculated from the deformation and strain of the window.

II. METHOD OF CALCULATION

The calculation of the elastic response of the window to applied pressure follows closely the method presented previously by Alt and Kalus.[1] The configuration of the window and its support are shown in Fig. 1. The elastic properties of a window composed of isotropic material are described by Young's modulus E and Poisson's ratio ν. The starting point for the calculation is the Navier equation for the displacement $\bar{u}$:[1,4,5]

$$(1-2\nu)\Delta\bar{u}+\bar{\nabla}(\bar{\nabla}\cdot\bar{u})=0. \tag{1}$$

The solution of this equation may be expressed in terms of an arbitrary biharmonic Galerkin vector $\bar{G}$,[4] where

$$\bar{u}E/(1+\nu)=2(1-\nu)\Delta\bar{G}-\bar{\nabla}(\bar{\nabla}\cdot\bar{G}). \tag{2}$$

In the case of cylindrical symmetry, the Galerkin vector has the special form $\bar{G}=Z(r,z)\hat{z}$, where Z may be written as a Fourier–Bessel expansion with the form[1]

$$\begin{aligned}Z=&\sum_{\alpha}\sin(\alpha z)[A'I_0(\alpha r)+B'\alpha rI_1(\alpha r)]+\cos(\alpha z)\\&\times[A''I_0(\alpha r)+B''\alpha rI_1(\alpha r)]\\&+\sum_{\gamma}J_0(\gamma r)[C'\sinh(\gamma z)+D'\gamma z\cosh(\gamma z)\\&+C''\cosh(\gamma z)+D''\gamma z\sinh(\gamma z)]+\sum_m Z_m,\end{aligned} \tag{3}$$

where J_m and I_m are Bessel functions and modified Bessel functions of order m, and Z_m are convenient, additional polynomial solutions of the biharmonic equation. One may choose $\alpha_n h/2$ and $\gamma_k d/2$ to be the nth and kth roots of $\sin(x)$ and $J_1(x)$, respectively. The problem is thus reduced to solving for numerical values of the coefficients of the Fourier–Bessel expansion of Z which will make $\bar{u}$ satisfy the boundary conditions.

The boundary conditions for the problem are the imposed stresses or displacements of the surfaces of the window. The displacements u_i may be expressed in terms of Z by the following equations:[5]

$$u_r=(1+\nu)[-\partial^2/\partial r\partial z]Z(r,z)/E, \tag{4a}$$

$$u_\theta=0, \tag{4b}$$

$$u_z=(1+\nu)[2(1-\nu)\nabla^2-\partial^2/\partial z^2]Z(r,z)/E. \tag{4c}$$

The strains ϵ_{ij} are given by $\epsilon_{rr}=\partial u_r/\partial r$, $\epsilon_{\theta\theta}=u_r/r$, $\epsilon_{zz}=\partial u_z/\partial z$, and $\epsilon_{rz}=(\partial u_r/\partial z+\partial u_z/\partial r)/2$. The stresses σ_{ij} are found by applying Hooke's law, $\sigma_{ij}=[\epsilon_{ij}+\delta_{ij}\epsilon_{kk}\nu/(1-2\nu)]E/(1+\nu)$, to obtain the expressions given by Eqs. (7) of Ref. 1.

The boundary conditions at the hydrostatically loaded top surface (rim) of the window are $\sigma_{zz}=-p_0$ ($\sigma_{rr}=-p_0$) and $\sigma_{rz}=0$. In the case that the center hole shrinks to zero, these hydrostatic boundary conditions also apply along the bottom window surface. The polynomial

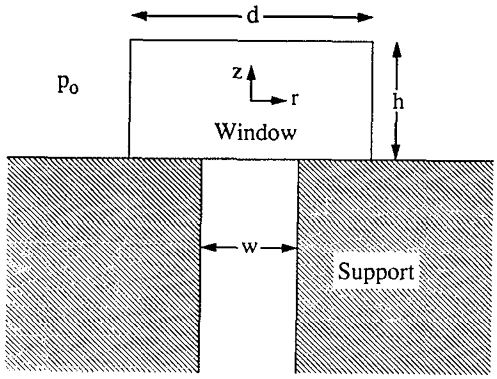

FIG. 1. Cross-sectional view of a Poulter window. The top surface is immersed in the high-pressure fluid while the bottom window surface rests against the support.

$$\sum_m Z_m = -p_0\{(5-4\nu)P_3(z) - 5(1-2\nu)P_2(r)P_1(z)\}/\{15(1+\nu)\}, \tag{5}$$

where P_m is the Legendre polynomial of order m, generates the hydrostatic solution in which the stress and strain tensors are diagonal, isotropic, and uniform with components $-p_0$ and $(-p_0/E)(1-2\nu)$, respectively. In the case that the loading is not hydrostatic along the bottom boundary, the deviation from the hydrostatic solution is represented by the terms of the Fourier–Bessel expansion.

It is most convenient to specify the boundary stress along the lower surface of the window. Then the set of simultaneous equations which result upon substitution of Eq. (3) for Z into the expressions for σ_{ij} can be split into two sets, each set having half as many unknown coefficients as the original set. One set contains the terms even in z and the other set has the odd terms. One only needs to match the boundary conditions along the bottom (or top) half of the window. These simplifications are not obtained with mixed boundary conditions. In any case, the equations for the boundary conditions are generated for a set of points along the boundary, and the least-squares solution for the coefficients of the truncated Fourier–Bessel expansion is obtained. The expansion for $Z(r,z)$ was truncated at 20 values of α_n and 40 values of γ_k, and the boundary equations were generated for 81 and 161 boundary points along the rim and bottom of the window.

It is known that $\sigma_{zz}=0$ along the bottom window surface for $r<w/2$ since the window is unsupported there. Also, one may assume vanishing shear stress along the entire bottom window surface if friction with the support is sufficiently low. However, the stress σ_{zz} along the window surface in contact with the support is unknown. The pressure exerted by the support is a function of the properties of the window and support materials, and the geometry of the window and the support. The support pressure could be obtained as a byproduct of a much more difficult calculation which solves for the elastic response of the window and the seat together. We have instead performed the simpler calculation which solves for the elastic response of the window alone, and have investigated a representative choice of forms for the support pressure function.

Uniform support pressure is the simplest possibility. The stress at the supported surface is then

$$\sigma_{zz} = -p_0[1-(w/d)^2]^{-1}, \tag{6}$$

where the stress is greater than the applied hydrostatic pressure because of the condition that the total force on top and bottom window surfaces must balance. This stress distribution would be obtained with a very stiff window resting on a very soft cylindrical seat of the same diameter. Uniform support pressure is obtained in this case because the deviation from flatness of the window and the conforming support surface under load is negligible compared to the longitudinal compression of the support (a window supported on a rubber O ring might approximate this case). Clearly, the other limiting case is that of a soft window resting on a perfectly rigid support. The boundary stress in this case will be sharply peaked at the inner rim of the support because the rigid support forces the bottom window surface to be sharply bent at the edge of the aperture when pressure is applied. A notion of the form of the boundary stress may be obtained by considering the case of an infinite medium (with $\nu=1/3$) containing a spherical cavity of radius R. When a uniaxial stress σ_{zz} is applied far from the cavity, the stress σ_{zz} in the equatorial plane of the cavity will be magnified by the factor $[1+(3/8)(R/r)^3 + (R/r)^5\}]$.[4] One may expect the stress near the edge of the support for a Poulter window to be even more sharply peaked because the window will try to bulge out through the hole in the support and bend down the edges of the support. The function

$$\sigma_{zz} = -p_0\left[1+a\left\{\sum_{m=1}^{6}\left(\frac{w}{2r}\right)^{2m+1}\right\}\right] \tag{7a}$$

with

$$a = \left\{2\sum_{m=1}^{6}\left[1-\left(\frac{w}{d}\right)^{2m-1}\right]\Big/(2m-1)\right\}^{-1} \tag{7b}$$

is found to produce an approximately flat supported surface to within a distance $d/40$ from the edge. The displacements of the window surfaces are compared in Fig. 2 for soft and hard support. Contour plots of the stress distribution inside the window are qualitatively similar for the two cases (Fig. 2 of Ref. 1 shows a typical stress distribution). While we do not know the exact form for the support pressure function for a particular choice of window and support, our two choices for the function represent the limiting cases. Unless the final results are very sensitive to the form of the support function, it will be sufficient to interpolate between the results for the limiting cases. These and subsequent calculations have been done using $\nu=0.168$ appropriate to fused silica glass.[6] The solution for a fused silica glass window resting on a stainless-steel sup-

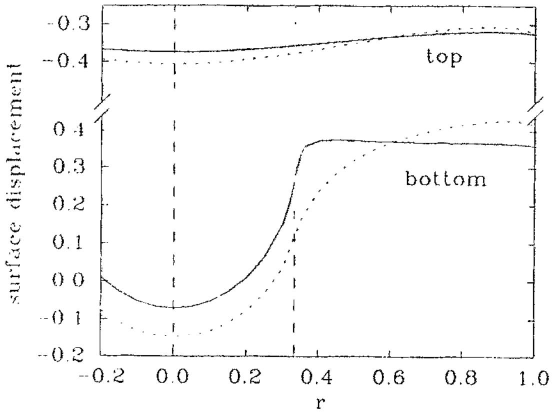

FIG. 2. Displacements $u_z(r)$ are shown for the top and bottom surfaces of a Poulter window with $d=2$, $h=1$, $w=d/3$, $\nu=0.168$, and $p_0/E=1$, in the limiting cases of a hard support [solid curve, support stress given by Eq. (7)] and a soft support [dashed curve, support stress given by Eq. (6)]. The window axis and the edge of the support are indicated by vertical dashed lines. For comparison, with hydrostatic loading the surface displacements would be ∓ 0.332 at $z=\pm h/2$. Note that the surface deformation has a larger amplitude with the soft support, but that the curvature of the bottom surface at $r=0$ and at the edge of the support is greater for the hard support. The support stress averaged over the support surface is 9/8 times the applied hydrostatic stress, and in the case of the hard support, the displacement of the window surface in contact with the support is very close to 9/8 times the hydrostatic value. In both cases the window bulges into the hole in the support when pressure is applied.

port ($E=72$ and 210 GPa, respectively)[7] is expected to be close to the solution we have calculated for the rigid support case.

Pressure applied to the window induces a change in the optical path length (OPL) for a ray traversing the window and a change in the optical thickness (OT) of the window.[8] There are two distinct contributions to the net optical effects due to applied pressure. First, the window surfaces are distorted and the geometrical thickness is altered. While the geometrical thickness decreases at all values of r, the thickness decreases least on axis because the window bulges out through the hole in the support. This constitutes a positive lens. Second, the compression of the window material alters its refractive index. For fused silica glass the refractive index increases with density, but the relative change in n is only 1/4 as large as the relative density change because of a compensating reduction of the atomic polarizability with compression.[6–11] Contour plots of the stress distribution inside the window show that there is a dome of reduced stress above the hole in the support. The refractive index of the material in this dome is not increased as much as in the surrounding material, and this constitutes a negative lens. The stress σ_{zz} makes the largest contribution to the negative lens because the contours of reduced σ_{zz} extend most deeply into the window (see Fig. 2 of Ref. 1). Since the geometric and refractive changes in the window due to applied pressure tend to cancel, not even the signs of the net optical effects can be determined without a careful calculation. In the simple case of a hydrostatically compressed fused silica window, the net effect of the competing contributions is to increase the optical path length but to decrease the optical thickness of the window (recall that the OPL is measured between two external fixed planes but that the OT is measured between the window surfaces).

The effects of strain on the optical properties of the window material are calculated by multiplying the strain-optical tensor by the nonzero strain components, adding this to the optical indicatrix of the unstrained isotropic glass, rotating to principal axis form, and inverting to obtain the dielectric tensor.[8] The anisotropy induced by the strain is small, and the lowest order result for the refractive index change for light propagating in the $\hat{z}$ direction and polarized in the $\hat{r}$ direction is

$$\Delta n_r = -(n_0^3/2)[p_{11}\epsilon_{rr} + p_{12}(\epsilon_{\theta\theta}+\epsilon_{zz})], \tag{8}$$

where n_0 is the refractive index of the unstrained glass, p_{ij} are elements of the strain-optic tensor,[6,8–11] and ϵ_{ij} are the strain components. For $\hat{\theta}$ polarized light, r and θ are interchanged in the above expression. Off the symmetry axis, the cylindrically symmetric strain field will result in an induced birefringence:

$$(n_r - n_\theta) = -(n_0^3/2)(p_{11}-p_{12})(\epsilon_{rr}-\epsilon_{\theta\theta}). \tag{9}$$

The net optical effect of the deformation and strain of the window is obtained by integrating the changes along the path of a ray traveling parallel to the z axis. To lowest order, the expressions for the changes in optical thickness and optical path length are

$$\Delta \mathrm{OT} = n_0 \Delta h + h \Delta \bar{n} \tag{10}$$

and

$$\Delta \mathrm{OPL} = (n_0 - 1)\Delta h + h\Delta \bar{n}, \tag{11}$$

where $\Delta \bar{n}$ is the average change in refractive index of the window material along the path of the ray. The pressure-induced focal power f^{-1} of the window is given by

$$f^{-1} = -(d^2/dr^2)\Delta \mathrm{OPL}\Big|_{r=0}, \tag{12}$$

where the focal length f is just the inverse of the focal power. Equation (11) ignores the effect of the increase in the refractive index Δn_g of the gas under pressure. Accounting for the refractive index of the gas adds a term

$$f_g^{-1} = \Delta n_g R_{\mathrm{top}}^{-1} \tag{13}$$

to the focal power given by Eqs. (11) and (12), where R_{top} is the radius of curvature of the top surface of the window. Except for very thin windows supported near the rim, where the curvature of the top surface becomes large and the other contributions to the focal power are near zero, f_g^{-1} is only a small correction to f^{-1}. The contribution given by Eq. (13) has not been included in the calculated results presented below. The results of our calculations are given in reduced units for a window of unit radius and unit stiffness, subjected to unit pressure; to obtain physical values one must multiply the reduced results by the appropriate factors of $(d/2)$ and (p_0/E).

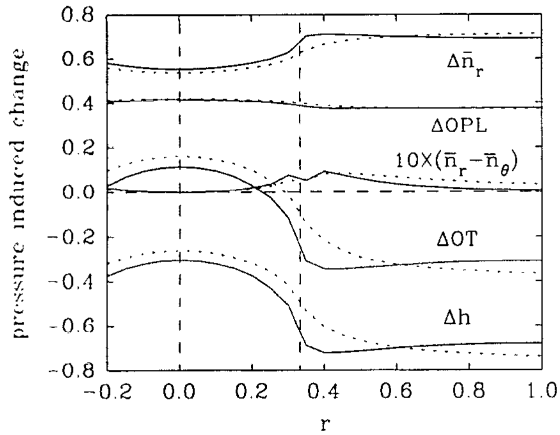

FIG. 3. Changes in the refractive index, optical path length, birefringence, optical thickness, and geometrical thickness (top to bottom in the diagram) are shown for a fused silica Poulter window with $d=2$, $h=1$, $w=d/3$, $\nu=0.168$, and $p_0/E=1$, in the limiting cases of hard support (solid curves) and soft support (dashed curves). The window axis and the edge of the support are indicated by vertical dashed lines. Each quantity is averaged or integrated along the path of a light ray parallel to the window axis at radius r. All parts of the window are compressed by the applied pressure, but the average compression is least along the axis. Thus, the refractive index has a minimum on axis, while the geometrical thickness has a maximum on axis. Their effects tend to cancel, resulting in a weak net positive lens (small curvature of ΔOPL, maximum at $r=0$) and a small net optical thickness change. The birefringence is maximum near the edge of the support and zero on axis.

TABLE I. Calculated results for a fused silica window, with $d=2$, $h=1$, and $w/d=1/3$, supported on a rigid seat. The assumed mechanical properties for fused silica are $E=72$ GPa and $\nu=0.168$ (Ref. 6), while the optical properties at $\lambda=632.8$ nm are taken as $n=1.46$, $p_{11}=+0.121$, and $p_{12}=+0.270$ (Ref. 9). Except for the birefringence, the values tabulated below correspond to the axial values of the solid curves shown in Figs. 2 and 3. As well as giving the dimensionless or reduced values which result from the calculation, the physical values are given for the specific case where $d=12$ mm and $p_0=100$ atm$=10.1$ MPa. Expressions for $\bar{n}$, $(\bar{n}_r-\bar{n}_\theta)$, ΔOT, ΔOPL, and f^{-1} are given by Eqs. (8)–(12).

Quantity	Reduced value	Physical value
Δn, top	0.714	1.01×10^{-4}
Δn, bottom	0.115	1.62×10^{-5}
$\Delta\bar{n}$	0.553	7.78×10^{-5}
$(\bar{n}_r-\bar{n}_\theta)_{\max}$	0.0091	1.28×10^{-6}
Δh	−0.301	−0.254 μm
ΔOT	0.113	0.095 μm
ΔOPL	0.414	0.350 μm
f^{-1}	0.316	0.741×10^{-2} m^{-1}
Curvature, top	0.355	0.833×10^{-2} m^{-1}
Curvature, bottom	3.796	8.904×10^{-2} m^{-1}

III. RESULTS AND DISCUSSION

Detailed results of the calculation are shown in Figs. 2 and 3 for a fused silica window with $h/d=1/2$ and $w/d=1/3$, for the limiting cases of soft [Eqs. (6)] and hard [Eq. (7)] support. With a soft support, the amplitude of the surface displacement is larger but the surface curvature at the edge of the support is reduced. On the axis, the main effect of a softer support is to increase the optical thickness of the window under pressure as a result of the more pronounced central bulge. The main qualitative features are essentially independent of the hardness of the support. Because the window bulges out into the hole in the support, the optical thickness of the window is increased on axis, even though it is decreased for the window directly above the supporting surface. The optical path length change is nearly constant across the face of the window because the variations in the $(n_0-1)\Delta h$ contribution to ΔOPL are 80% cancelled by the variations in the $h\Delta\bar{n}$ contribution. Table I summarizes the quantitative results for this fused silica window on a rigid support, in reduced units and also for the specific case of a window 12 mm in diameter and subjected to a pressure of 100 atm. The lens induced under pressure, with a focal length of 135 m, is very weak as a result of the fortuitous cancellation of terms. If a similar calculation is done for a sapphire window viewed along its c axis (ignoring the small mechanical anisotropy), one obtains a lens which is twice as strong even though sapphire is five times stiffer than silica.[7,9,12] The cancellation of terms is less complete in the calculation of the optical thickness, and in this case the OT change is three times smaller for sapphire, as one might expect due to its much higher stiffness. The effect of a weak pressure-induced lens on the results of gas-phase nonlinear-optical measurements[2] is of order z_0/f, where z_0 is the confocal parameter of the focused laser beam in the cell and f is the focal length of the pressure-induced lens. The experimental corrections are only of order 0.1% because of the fortuitously weak lensing for fused silica windows.

The variation of focal power and the optical thickness change as functions of the window thickness and the diameter of the central hole in the support, for a fused silica window, are shown in Figs. 4 and 5. In the limit $w/d\rightarrow1$, the results depend only on the thickness of the window. A thin window supported near its edge will give near zero lensing because it is simply bent so that the stress distribu-

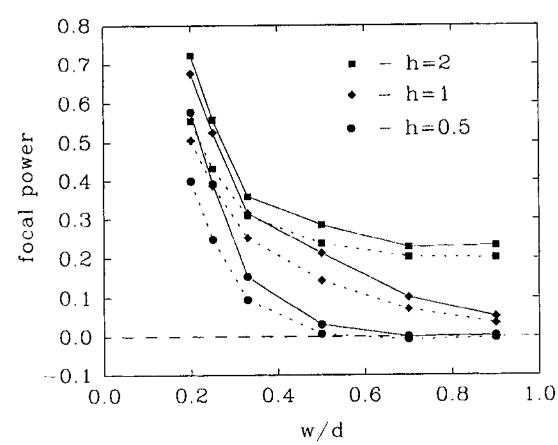

FIG. 4. The pressure-induced focal power f^{-1} of a fused silica Poulter window with $d=2$ and $p_0/E=1$ is shown for a range of thickness h and clear aperture w, for the limiting cases of hard support (solid curves) and soft support (dashed curves). The focal power of the window is reduced by making it thinner or by increasing the diameter of the hole in the support, but this also lowers the breaking pressure of the window (Ref. 1). The focal power of the window increases as the support is made stiffer, the effect being more pronounced for small w/d. As w/d decreases below 0.2, f^{-1} will reach a maximum, become independent of h, and finally tend to zero at $w=0$.

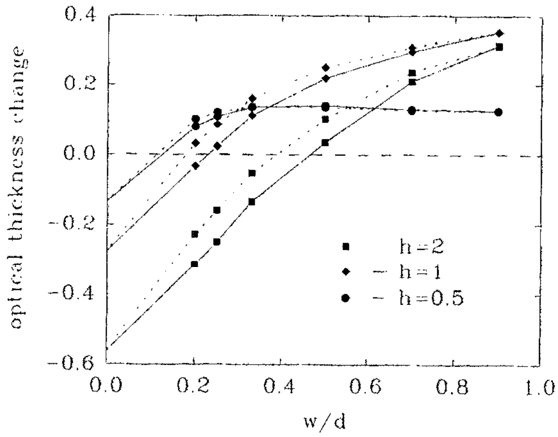

FIG. 5. The pressure-induced change in axial optical thickness ΔOT of a fused silica Poulter window with $d=2$ and $p_0/E=1$ is shown for a range of thickness h and clear aperture w, for the limiting cases of hard support (solid curves) and soft support (dashed curves). The value of ΔOT goes through zero for $w/h \approx 0.4$, but a thick window is needed to reach this compensation point unless the clear aperture is made very small. For thin windows and large apertures, the optical thickness increases under pressure even though the geometrical thickness of the window decreases. When $w=0$, so that the window is hydrostatically compressed, the optical thickness decreases under pressure.

tion and thickness are almost independent of r. In the limit $w/d \to 0$, the focal power becomes independent of thickness and tends to zero for $w/d=0$. The accuracy of the calculated results becomes more sensitive to the number of terms in the expansion as the value of w/d is reduced, and for this reason we did not compute results for $w/d<0.2$. The optical thickness change, in the limit $w/d \to 0$, will tend to the value that would be obtained with pure hydrostatic loading.

$$\Delta\mathrm{OT}\Big|_{w=0} = n_0 h(1-2\nu)[1-(n_0^2/2)(p_{11}+2p_{12})] \times(-p_0/E), \tag{14}$$

which is about $-0.29h$ in reduced units. The dependence of ΔOT on h in the limit $w/d \to 1$ is more complicated, having an extremun for $h/d \simeq 1/2$. For a thin window with $w>h$, ΔOT is nearly independent of w/d. For a thick window, increasing w decreases focal power but increases ΔOT.

While the pressure-induced change in laser beam focusing turns out to be relatively small, the pressure-induced change in window transmission can be large. One contribution to the transmission change is due to changes in the refractive index of the window material at the top and bottom surfaces (see Table I). This alters the Fresnel reflection coefficients of the surfaces, but the resulting transmission changes are only of order 0.01%. Gross transmission changes can occur, however, if the reflections from the top and bottom window surfaces are allowed to interfere. For light of wavelength 400 nm, the ΔOT given in Table I will result in an additional $\lambda/2$ phase shift between the two reflected waves. The effect of this phase shift depends on the initial phase difference between the reflections, but in the worst case the change in the transmission coefficient of the window of the gas cell will be $\pm 4(n_0-1)^2/(n_0+1)^2$. For a fused silica window without antireflection coatings, the transmission change could be as large as 15% when pressure is applied. Even with good antireflection coatings, the transmission change could be of order 1%. This very objectionable "étalon fringe" effect can be avoided by using windows with a small wedge angle between the top and bottom surfaces. For narrow beams, the wedge should be large enough to ensure that the reflected beams do not overlap.

The birefringence induced under pressure may significantly alter the polarization state of a laser beam transmitted through the window. The peak birefringence of the specific window presented in Table I will result in a retardation of 90 mrad and an extinction ratio of 2×10^{-3}. However, since the birefringence varies approximately quadratically with distance from the axis, the effect of the induced bifrefringence of the stressed window on the polarization state of a narrow beam can be minimized by centering the narrow beam on the window axis. For example, the extinction ratio for the window in Table I will remain below 10^{-6} for a centered, 0.5-mm-diam light beam.

In summary, the confocal parameter, power, and polarization of a laser beam transmitted through a Poulter window will be altered when pressure is applied to the window. These effects are not negligible for nonlinear-optical measurements of the highest accuracy because of the strong dependence of the measured signal on incident light intensity and polarization. The analysis of the results of high-pressure gas-phase nonlinear-optical experiments can be corrected for these effects using the quantitative estimates of the optical properties of stressed windows which have been presented above. These results may also be a useful guide in the design of experiments for other critical optical measurements of compressed gases.

[1] H. C. Alt and J. Kalus, Rev. Sci. Instrum. **53**, 1235 (1982).
[2] D. P. Shelton, Phys. Rev. A **42**, 2578 (1990).
[3] E. Whalley, A. Lavergne, and P. T. T. Wong, Rev. Sci. Instrum. **47**, 845 (1976).
[4] L. D. Landau and E. M. Lifshitz, *Theory of Elasticity*, 3rd ed. (Pergamon, Oxford, 1986).
[5] H. Leipholz, *Theory of Elasticity* (Noordhoff, Leyden, 1974).
[6] N. F. Borrelli and R. A. Miller, Appl. Opt. **7**, 745 (1968).
[7] R. M. Tennent, *Science Data Book* (Oliver and Boyd, Edinburgh, 1971).
[8] Guenther, *Modern Optics* (Wiley, New York, 1990).
[9] R. W. Dixon, J. Appl. Phys. **38**, 5149 (1967).
[10] K. Vedam, E. D. D. Schmidt, and R. Roy, J. Am. Ceram. Soc. **49**, 531 (1966).
[11] W. Primak and D. Post, J. Appl. Phys. **30**, 779 (1959).
[12] J. Reintjes and M. B. Schulz, J. Appl. Phys. **39**, 5254 (1968).